
Article:
Hope, Alexander, Croze, Ottavio A., Poon, Wilson et al. (2016) Resonant alignment of microswimmer trajectories in oscillatory shear flows. Physical Review Fluids. 051201. pp. 1-8. ISSN: 2469-990X

https://doi.org/10.1103/PhysRevFluids.1.051201

Resonant alignment of microswimmer trajectories in oscillatory shear flows

Alexander Hope,[1] Ottavio A. Croze,[2,*] Wilson C. K. Poon,[3] Martin A. Bees,[4] and Mark D. Haw[1]

[1] *Department of Chemical and Process Engineering, University of Strathclyde, James Weir Building, 75 Montrose Street, Glasgow G1 1XJ, United Kingdom*
[2] *Cavendish Laboratory, University of Cambridge, Cambridge, CB3 0HE, United Kingdom*
[3] *SUPA and The School of Physics & Astronomy, The University of Edinburgh, Kings Buildings, Mayfield Road, Edinburgh EH9 3JZ, United Kingdom*
[4] *Department of Mathematics, University of York, York YO10 5DD, United Kingdom*

(Dated: August 4, 2016)

Oscillatory flows are commonly experienced by swimming microorganisms in the environment, industrial applications and rheological investigations. We experimentally characterise the response of the alga *Dunaliella salina* to oscillatory shear flows, and report the surprising discovery that algal swimming trajectories orient perpendicular to the flow-shear plane. The ordering has the characteristics of a resonance in the driving parameter space. The behaviour is qualitatively reproduced by a simple model and simulations accounting for helical swimming, suggesting a mechanism for ordering and criteria for the resonant amplitude and frequency. The implications of this work for active oscillatory rheology and industrial algal processing are discussed.

PACS numbers: Valid PACS appear here

Many swimming microorganisms experience shear flow in natural and industrial processes. Swimming is strongly biased by environmental cues and fluid shear [1, 2], with significant implications for ecology [3] and industrial exploitation [4]. Classic examples include directed swimming relative to light (phototaxis) and hydrodynamic focusing in down-welling flow due to viscous and gravitational torques (gyrotaxis) [1, 5].

There is great potential to use individual and collective microswimmer behaviour to improve microbial biotechnology, such as algal photobioreactor design [4]. For example, gyrotactic microorganisms in laminar channel flow tend to focus and so drift faster and diffuse less than non-swimming cells or nutrients [6, 7] while in turbulent flows cells accumulate in transiently downwelling [7–9] or strongly accelerated [10] regions. Horizontal shear flows can trap gyrotactic swimmers (a mechanism for oceanic thin layers) [3] and modify hydrodynamic instabilites and patterns (bioconvection) [11, 12]. Phototaxis and shear flow can combine to drive cell focusing [13] and pattern formation [14]. Complex transport dynamics can even result from relatively simple shear flow [2, 15]. The rheology of active media is also of recent interest: suspensions of swimming bacteria behave less viscously [16] and algae more viscously [17] than dead cells.

Here, we investigate the interaction of the swimming alga *Dunaliella salina* with oscillatory shear flows. Surprisingly, in experiments swimming trajectories are strongly ordered by the flow for particular driving parameter values. The ordering mechanism is distinct from that observed recently with *Dunaliella primolecta*, with constant, strong shear flows [18]. We explore the observed resonant ordering employing simple but predictive models, and discuss implications for active oscillatory rheology and industrial processing of swimming algae.

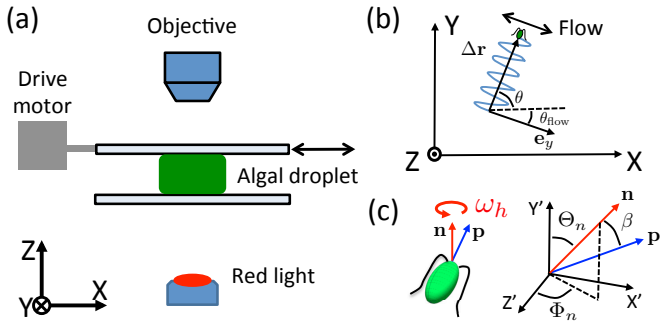

FIG. 1. (a) Oscillatory flow and imaging setup. (b) Trajectories orientations θ from the x-axis are evaluated from their displacements $\Delta\mathbf{r}$. The flow axis $\mathbf{e}_y$ was often rotated by θ_{flow} from x (consistent across repeat experiments). (c) *Dunaliella salina* swimming and helical rotation directions, $\mathbf{p}$ and $\mathbf{n}$; model coordinate system and angles (see text).

D. salina CCAP 19/18 cells (long axis $\approx 15\,\mu$m) were grown on modified Pick medium [19, 20] under 12:12 light/dark cycle at 21°C. All experiments were carried out at this temperature. Cells were concentrated by upswimming (gravitaxis) using cotton wool rafts [11]. Dilute (10^6 cells/ml) suspensions were subjected to oscillatory shear on the stage of an optical microscope (Olympus BX51). The suspension was placed between two transparent parallel plates 400 μm apart, the top plate connected to an electromechanical drive that sinusoidally sheared the suspension (Fig. 1). Plate parallelism was ensured by zeroing sample capillary flow. Video sequences (100-400 Hz) of sheared algae were acquired using a Mikrotron MC1310 at 10× (NA 0.25) using red-filtered bright-field illumination to minimise phototaxis [21]. Sequences were captured in a plane equidistant from top and bottom plates at depth 200 μm. Algae were tracked using MATLAB versions of established

algorithms [22, 23]. The direction of the imposed oscillating flow was inferred from short-time cell trajectories and confirmed by tracking PEGylated polystyrene colloids (Supplementary Materials, Fig. S1). Cell observation before and after measurements found that the apparatus did not damage the cells (e.g. deflagellation).

With no flow, *D. salina* swimming trajectories were distributed isotropically in the horizontal plane (Fig. 2a). As in [24], gravitactic bias was not evident for tracks in this plane on experimental timescales. On application of oscillatory shear with amplitude A and frequency f trajectories might be expected simply to reflect superposition of isotropic swimming and oscillatory advection. This was indeed the case for some driving parameters, such as $A = 240$ μm and $f = 6$ Hz (Fig 2b). However, for $A = 448$ μm and $f = 2$ Hz swimming trajectories unexpectedly aligned perpendicular to the flow-shear plane (Fig. 2c). Alignment can be quantified by the start-to-end displacement, $\Delta\mathbf{r}(\tau)$, of each swimmer trajectory (Fig. 1b). Evaluated at short times within a cycle, $\Delta\mathbf{r}(\tau)$ provides the flow direction $\mathbf{e}_y \sim \Delta\mathbf{r}(\tau \to 0)$. However, evaluating $\Delta\mathbf{r}(\tau)$ over the largest available integer multiple n of the oscillation period, $\tau = n/f$, provides overall trajectory orientation, θ, and speed, $v_t = |\Delta\mathbf{r}|/\tau$.

Distributions $P(\theta)$ of orientations are presented beside the trajectories in Fig. 2. The distribution for $f = 2$ Hz, $A = 448$ μm shows how trajectories orient along the line perpendicular to the flow-shear plane, but are equally likely in either direction along this line. If the flow is halted, the distribution returns to uniform (Fig. S1, Supplementary Materials). Speed distributions for aligned trajectories (Fig. 2c) are similar to those without flow (Fig. 2a). These reflect the swimming speed distribution [25]. Hence, swimmers in aligned trajectories travel perpendicular to the flow at their swimming speed (but very slow swimmers cannot make much progress, biasing the distribution towards high speeds in Fig. 2c). Without alignment (Fig. 2b), the speed distribution reflects contributions by swimming and the oscillatory flow, which accounts for the bias towards low speeds.

To statistically quantify observed alignment as a function of the flow parameters, we count trajectories with displacement $\Delta\mathbf{r}$ oriented perpendicular, $N_\perp$, and parallel, $N_\parallel$, to the flow direction and define $R = N_\perp/N_\parallel$. By parallel (perpendicular) displacements we mean swimming orientations within $\pm\pi/4$ of the flow (vorticity) axis. We also provide the alternative measure $r = (\langle\sin(\theta - \theta_{flow})\rangle^2 + \langle\cos(\theta - \theta_{flow})\rangle^2)^{1/2} \in [0, 1]$, where averages are over all angles (which were doubled for axial distributions at resonance) [26]. Small r denotes isotropy, large r alignment (see Fig. 2). The surface plot in Fig. 3 illustrates how the alignment has the characteristics of resonance, occupying a small region of the imposed flow parameter space. Fixed amplitude and frequency sections of the ordering surface are shown in Fig. 4 and discussed below.

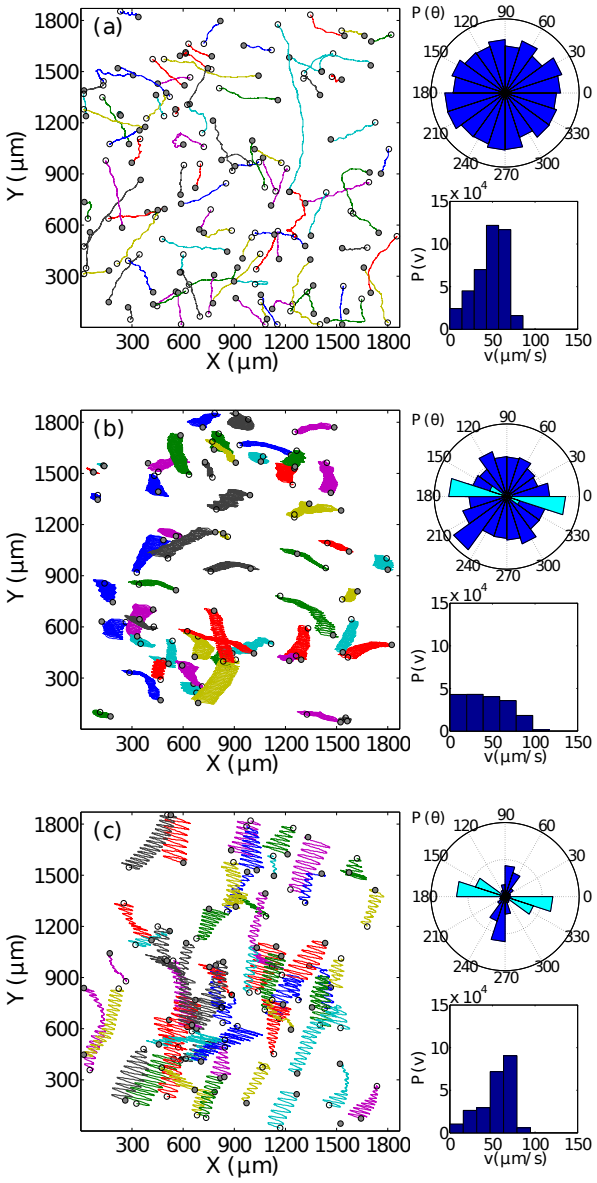

FIG. 2. Trajectories, orientation and speed distributions of *D. salina*. (a) No flow: isotropic trajectories (alignment measures [$r = 0.02$, $R = 0.9$], see text). (b) Oscillatory shear flow with amplitude $A = 240$ μm and frequency $f = 6$ Hz: tracks show oscillation (cyan) at short times, but are isotropic (blue) at longer times [$r = 0.05, R = 1.6$]. (c) $A = 448$ μm and $f = 2$ Hz: swimming directions align perpendicular (blue) to the flow oscillation direction (cyan) [$r = 0.53, R = 4.4$]. Open/closed circles denote start/end points of each 2.5s track.

Discussion. The observed trajectories result from the combination of shear flow and swimming. Many algae swim helically, in part to facilitate phototaxis via a directional eyespot [27]. Thus we model the algae as helical swimmers in a flow. Following [28], we assume that a cell at position $\mathbf{r}$ swimming with speed v in direction $\mathbf{p}$ has an intrinsic angular velocity $\omega_h\mathbf{n}$ about an axis

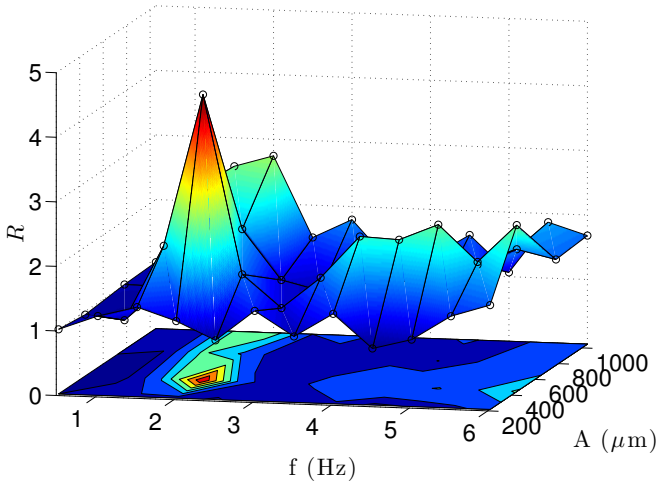

FIG. 3. Alignment ratio R as a function of driving amplitude A and frequency f for oscillatory flow in a shear cell with $H = 400\ \mu$m gap width. A is a measure of horizontal displacement.

$\mathbf{n}$, where $\mathbf{p}\cdot\mathbf{n} = \cos\beta$, for constant angle β, due to an asymmetric (non-planar) flagellar stroke. Hence, if the only external torque is due to flow with velocity $\mathbf{u}$ and vorticity $\boldsymbol{\omega}$, spherical swimmers obey $\dot{\mathbf{r}} = \mathbf{u}(t) + v\mathbf{p}$, $\dot{\mathbf{p}} = \left(\frac{1}{2}\boldsymbol{\omega}(t) + \omega_h\mathbf{n}\right)\times\mathbf{p}$ and $\dot{\mathbf{n}} = \frac{1}{2}\boldsymbol{\omega}(t)\times\mathbf{n}$. Experimental observations suggest that the fluid velocity is $\mathbf{u}(t) = \dot{\gamma}_\infty Z\cos(\omega_d t)\mathbf{e}_x$, with vorticity $\boldsymbol{\omega}(t) = \dot{\gamma}_\infty\cos(\omega_d t)\mathbf{e}_y$. Here $\mathbf{e}_x$ and $\mathbf{e}_y$ are along the positive flow and vorticity directions, respectively, $\dot{\gamma}_\infty = \omega_d A/H$ is the maximum shear rate and $\omega_d = 2\pi f$ is the angular driving frequency (recall A, f and H are driving amplitude, frequency and gap width, respectively). Nondimensionalising lengths with A and times with $1/\omega_d$, the model equations read

$$\dot{\mathbf{r}} = \Gamma\cos(t)Z\mathbf{e}_x + \nu\mathbf{p} \tag{1}$$

$$\dot{\mathbf{p}} = \left[\frac{\Gamma}{2}\cos(t)\mathbf{e}_y + \Omega^{-1}\mathbf{n}\right]\times\mathbf{p};\ \ \dot{\mathbf{n}} = \frac{\Gamma}{2}\cos(t)\mathbf{e}_y\times\mathbf{n} \tag{2}$$

where $\Gamma = \dot{\gamma}_\infty/\omega_d = A/H$ is the dimensionless shear rate/amplitude, $\Omega = \omega_d/\omega_h$ is a frequency ratio and $\nu = v/(A\omega_d) = \nu_0/(\Gamma\Omega)$ a nondimensional swimming speed, with $\nu_0 = v/(\omega_h H)$. The Cartesian representation of (1-2), with Z measured from the bottom plate and XY the flow-vorticity plane (Fig. 1), was solved numerically to simulate a suspension of swimmers (see Supplementary Materials). The ratio R was computed from many simulations with a uniform distribution of initial swimmer orientations.

Non-swimmers ($\nu = 0$) passively follow the imposed oscillatory flow. In the absence of flow, the governing equations predict helical trajectories: $\mathbf{p}$ rotates around $\mathbf{n}$ (the helix axis) with frequency ω_h. With the experimental resonance close to helical swimming frequency, it is tempting to think that helical trajectories are responsible for the observed alignment. This is only partially true, as we shall see.

First we ask if the combination of 'non-helical' swimming and oscillatory shear alone is sufficient to induce ordering in experiment. Fig. 4 displays the ordering ratio (experiment a,b; simulation c,d) and simulated swimmer trajectories (e) for a model where helical swimming is switched off (dashed lines). While R peaks at characteristic values of the driving amplitude Γ (Fig 4c), it is entirely independent of driving frequency (Fig 4d) in stark contrast to the experiments. The non-helical limit does, however, predict alignment: it is worth considering further. When $\beta = 0$, the governing equations simplify considerably if we choose Euler angles Θ and Φ (Fig. 1c) such that $\mathbf{p} = \mathbf{n} = (\sin\Theta\sin\Phi, \cos\Theta, \sin\Theta\cos\Phi)$, where Θ increases from the direction of vorticity, $\mathbf{e}_y$, along the Y-axis, and Φ is measured from the Z-axis [e.g. $(\Theta, \Phi) = (\pi/2, \pi/2)$ is along the X-axis]. Equations (1-2) give

$$\dot{X} = \nu_\perp\sin\Phi + \Gamma\cos(t)Z \tag{3}$$

$$\dot{Y} = \nu_\parallel \tag{4}$$

$$\dot{Z} = \nu_\perp\cos\Phi \tag{5}$$

$$\dot{\Theta} = 0;\ \ \dot{\Phi} = \frac{\Gamma}{2}\cos(t) \tag{6}$$

where $\nu_\perp = \nu\sin\Theta_0$ and $\nu_\parallel = \nu\cos\Theta_0$ are the nondimensional swimming speed components perpendicular and parallel to $\mathbf{e}_y$. Integration of (4) and (6) yields $Y(t) = Y_0 + \nu_\parallel t$, $\Theta(t) = \Theta_0$ and

$$\Phi(t) = \Phi_0 + \frac{\Gamma}{2}\sin(t). \tag{7}$$

(Recall that $\Gamma = A/H$ is the non-dimensional shear rate.) As the Y component of the trajectory grows linearly in time, independent of shear, alignment can only depend on the coupled X and Z dynamics. In particular, closed orbits in the XZ-plane are present at resonance, see Fig. 4e, panel (i). For such orbits, progress only in the Y-direction is possible, leading to alignment. Off-resonance, orbits are open and cells can progress in X and Z directions (Fig. 4e, panel (ii)).

This phenomenology can be understood in terms of oscillatory Jeffery dynamics of the swimmer orientation. We see from (7) that oscillatory shear forces swimmer orientation in the vertical XZ-plane to describe circular arcs swept sinusoidally in time (contrast this with circular Jeffery orbits in steady shear flow, $\omega_d \to \infty$), with angular amplitude $\Gamma/2$. Folded orbits only arise when shear is sufficiently large to rotate swimmer orientation by integral multiples of π, so it can make no net progress during a cycle (see 4e). This provides a prediction for the resonant ordering amplitude $\Gamma_{\rm res} \approx 2\pi n$, $n \in \mathbb{Z}$, in good agreement with non-helical simulations (Fig 4c). The latter agree qualitatively with the experimental results in Fig 4a. Quantitatively, much smaller values of Γ are sufficient to induce ordering in experiment. A possibility is that the Γ reported underestimates the shear swimmers were exposed, e.g. because the intrinsic flagellar beats cause effective cell shape changes leading to

unexpected response to shear [29, 30]. Alternatively, additional mechanisms, such as those discussed below, are at play to modify the ordering dynamics.

The model for non-helical swimmers predicts alignment as a function of amplitude, but does not reproduce the experimentally observed dependence on both driving amplitude *and* frequency (Fig 4b). *D. salina* is a helical swimmer, rotating at $1.5-2$ Hz [25]. This second, internal frequency provides the possibility of further resonance. Indeed, with $\beta \neq 0$ (recall β is the angle between $\mathbf{p}$ and $\mathbf{n}$) numerical results reveal that ordering is frequency dependent (Fig. 4d). Position equations are unchanged, but depend on more complex orientation dynamics resulting from the coupling of flow-induced and helical rotation. Cell orientation angles Θ_p and Φ_p, defining $\mathbf{p}$, evolve according to (see Supplementary Materials)

$$\dot{\Theta}_p = \Omega^{-1} \sin\Theta_n \sin(\Phi_n - \Phi_p), \tag{8}$$

$$\dot{\Phi}_p = \frac{\Gamma}{2}\cos(t) + \Omega^{-1}\left[\cos\Theta_n - \sin\Theta_n \cot\Theta_p \sin(\Phi_n + \Phi_p)\right], \tag{9}$$

whereas angles for $\mathbf{n}$ satisfy (6), such that $\dot{\Theta}_n = 0$, $\dot{\Phi}_n = \Gamma\cos(t)/2$. As the $\mathbf{p}$-dynamics are slaved to the $\mathbf{n}$-dynamics, trajectories with helical swimming do retain broad features of non-helical orbits in oscillatory shear, see Fig. 4e, but they are nevertheless qualitatively perturbed (even for infinitesimal β). Thus only for particular driving frequencies and amplitudes does helical swimming produce alignment-inducing orbits. The frequency condition for ordering can be obtained by considering the case of a swimmer with $\mathbf{n}$ in the direction of vorticity: $\Theta_n(0) = 0 = \Phi_n(0)$; $\Theta_p(0) = \beta$; and $\Phi_p(0) = 0$. Equation (9) then integrates to $\Phi_p(t) = \frac{\Gamma}{2}\sin(t) + \Omega^{-1}t$: a helical phase can perturb simple Jeffery rotation by the flow. Only when $\Omega \sim 1$, i.e. when the driving and helical phase are synchronised, can a resonant value of Γ give alignment, agreeing with both simulations and experiments (Fig 4b,d).

Oscillatory Jeffery orbits and helical swimming provide a first order explanation for the dependence of resonance in experiments on both frequency and amplitude. The model is predictive: helical frequency shifts alter resonant alignment, e.g. simulations of the predatory dinoflagellate *Pfiesteria piscida* (Supplementary Materials) predict a resonant frequency shift when helical frequency increases in the presence of prey (Fig 4d, inset). This description could be extended to investigate how additional effects such as taxes, orientation noise, inertia and cell shape either dominate, compete or act in concert with helical swimming to affect resonance. Intriguing possibilities include stochastic resonance due to noise in the flow velocity gradients [31] and the aforementioned effective shape due to flagellar beats [29, 30]. The possibility of flagellar deformation by shear [2] seems unlikely. Shear rates on the same order as our experiments can modify flagellar dynamics for cells held on a micropipette

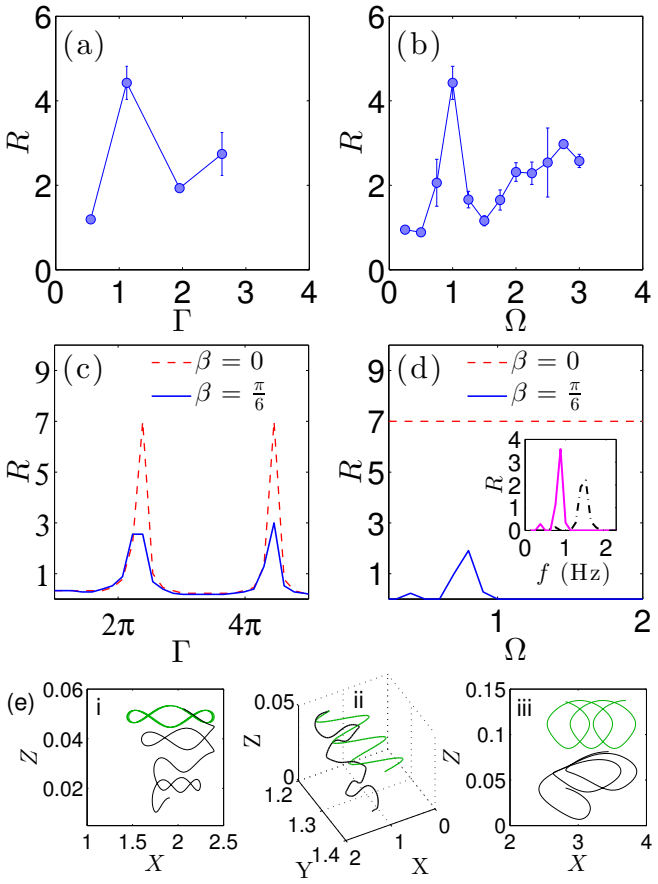

FIG. 4. Alignment ratio R vs. amplitude Γ and frequency Ω from experiment (errorbars smaller than data points not shown) (a, b) and simulation (c, d). Simulation predictions are shown with ($\beta = \pi/6$, solid) and without ($\beta = 0$, dashed) helical swimming (frequency $f_h = 2$Hz), only the latter providing frequency dependence. Trajectories ($\beta = 0$, green; $\beta = \pi/6$, black) are also shown in (e): at resonance, $[\Gamma, \Omega] = [7.5, 0.75]$, for XZ plane (i) and 3D views (ii); off-resonance $[\Gamma, \Omega] = [4, 0.75]$ (iii). Only trajectories closed in XZ provide ordering. Inset of (d): simulations of *P. piscida* in oscillatory flow, which increases its helical frequency from 1 (solid line) to 2 Hz (dash dot) when predating [33]. We predict a measureable shift in the resonance peak.

[32]. However, our cells are in suspension (free to rotate): much larger shear will be necessary to deform their flagella. A full analytical investigation of the nonlinear dynamics of the helical model in oscillatory shear is beyond the scope of this paper, but it is clear that much is to be discovered, analogous to structures observed for swimming cells in Poiseuille flow [15].

Conclusions. We have demonstrated the surprising response of swimming microalgae to oscillatory shear flows, producing an alignment of trajectories with a set of resonance peaks in the parameter space of driving frequency and amplitude. A simple model combining shear and non-helical swimming predicts resonant alignment of the trajectories of swimming cells, but only when helical

swimming is included does the experimentally observed frequency dependence of the resonance arise. The rich dynamics and the counterintuitive interactions between swimmers and flow revealed by our experiments and modelling have implications for both active suspension rheology and the design of novel cell processing methods. While simplified models of swimmers (rod or spheroidal pushers and pullers with no helical motion) appear adequate to explain active rheological phenomena such as shear-thickening in algal suspensions [17, 34], the current work suggests such models may fail in active *oscillatory* rheology experiments. Biotechnologically, the results hint at methods for improvement in efficiency of the algal processing pipeline [35]. For example, in downstream processing of useful microalgae, like the β-carotene producer *D. salina*, cells commonly experience oscillatory flows. Resonant alignment will provide boundary accumulation over times L/v, where L is the size of the shear plate and v is the swimming speed. This may be 'engineered out' by tuning process parameters from resonance; or it may be fruitfully exploited as a new way to guide and harvest cells.

We thank A. Schofield for providing colloids. OAC, WCKP, MDH and MAB acknowledge support from the Carnegie Trust for the Universities of Scotland, the Winton Programme for the Physics of Sustainability (OAC) and Leverhulme Trust (MDH). OAC and MAB acknowledge an EPSRC mobility grant (EP/J004847/1), WCKP the Programme Grant (EP/J007404/1) and ERC Advanced Grant (ADG-PHYAPS).

* oac24@cam.ac.uk

[1] T. J. Pedley and J. O. Kessler, Annu. Rev. Fluid Mech. **24**, 313 (1992).
[2] R. Rusconi and R. Stocker, Curr. Opin. Microbiol. **25**, 1 (2015).
[3] W. M. Durham, J. O. Kessler, and R. Stocker, Science **323**, 1067 (2009).
[4] M. A. Bees and O. A. Croze, Biofuels **5**, 53 (2014).
[5] N. A. Hill and T. J. Pedley, Fluid Dyn. Res. **37**, 1 (2005).
[6] R. Bearon, M. A. Bees, and O. A. Croze, Phys. Fluids (2012).
[7] O. A. Croze, G. Sardina, M. Ahmed, M. A. Bees, and L. Brandt, J. R. Soc. Interface **10**, 20121041 (2013).
[8] W. M. Durham, E. Climent, M. Barry, F. D. Lillo, G. Boffetta, M. Cencini, and R. Stocker, Nat. Commun. **4**, 3148 (2013).
[9] C. Zhan, G. Sardina, E. Lushi, and L. Brandt, J. Fluid Mech. **739**, 22 (2014).
[10] F. De Lillo, M. Cencini, W. M. Durham, M. Barry, R. Stocker, E. Climent, and G. Boffetta, Phys. Rev. Lett. **112**, 044502 (2014).
[11] O. A. Croze, E. E. Ashraf, and M. A. Bees, Phys. Biol. **7**, 046001 (2010).
[12] Y. Hwang and T. J. Pedley, J. Fluid Mech. **738**, 522 (2014).
[13] X. Garcia, S. Rafaï, and P. Peyla, Phys. Rev. Lett. **110**, 138106 (2013).
[14] C. R. Willams and M. A. Bees, J. Fluid Mech. **678**, 41 (2011).
[15] A. Zöttl and H. Stark, Phys. Rev. Lett. **108**, 218104 (2012).
[16] A. Sokolov and I. S. Aranson, Phys. Rev. Lett. **103**, 148101 (2009).
[17] S. Rafaï, L. Jibuti, and P. Peyla, Phys. Rev. Lett. **104**, 098102 (2010).
[18] A. Chengala, M. Hondzo, and J. Sheng, Phys. Rev. E **87**, 052704 (2013).
[19] U. Pick, L. Karni, and M. Avron, Plant Physiol. **81**, 92 (1986).
[20] J. Polle, private communication.
[21] V. A. Martinez, R. Besseling, and O. A. C. *et al.*, Biophys. J. **103**, 1637 (2012).
[22] M. Kilfoil lab software research tools `http://people.umass.edu/kilfoil/downloads.html`.
[23] J. Crocker and D. G. Grier, J. Colloid Interface Sci. **179**, 298 (1996).
[24] N. A. Hill and D.-P. Häder, J. Theor. Biol. **186**, 503 (1997).
[25] O. A. Croze *et al.*, in preparation.
[26] K. V. Mardia and P. Jupp, *Directional Statistics* (John Wiley and Sons, 2000).
[27] K. W. Foster and R. D. Smyth, Microbiol. Rev. **44**, 572 (1980).
[28] R. N. Bearon, J. Math. Biol. **66**, 1341 (2013).
[29] S. O'Malley and M. A. Bees, Bull. Math. Biol. **74**, 232 (2012).
[30] L. Jibuti, W. Zimmermann, S. Rafaï, and P. Peyla, ArXiv preprint (2014).
[31] F. Guzmán-Lastra and R. Soto, Phys. Rev. E **86**, 037301 (2012).
[32] G. S. Klindt, C. Ruloff, C. Wagner, and B. M. Friedrich, ArXiv preprint (2016).
[33] J. Sheng, E. Malkiel, J. Katz, J. Adolf, R. Belas, and A. R. Place, Proc. Natl. Acad. Sci. USA **104**, 17512 (2007).
[34] M. C. Marchetti, J. F. Joanny, T. B. Liverpool, J. Prost, M. Rao, and R. A. Simha, Rev. Mod. Phys. **85**, 1143 (2015).
[35] S. A. Scott, M. P. Davey, J. S. Dennis, I. Horst, C. J. Howe, D. J. Lea-Smith, and A. G. Smith, Curr. Opin. Biotechnology **21**, 277 (2010).